Chapter 2

Mathematical Modelling of Residual Stresses

2.1 Introduction

Grinding is approximated as an iso-thermal and two-dimensional problem with plane-strain deformation. The interaction between a grinding wheel and a workpiece surface is shown in Fig. 2.1.

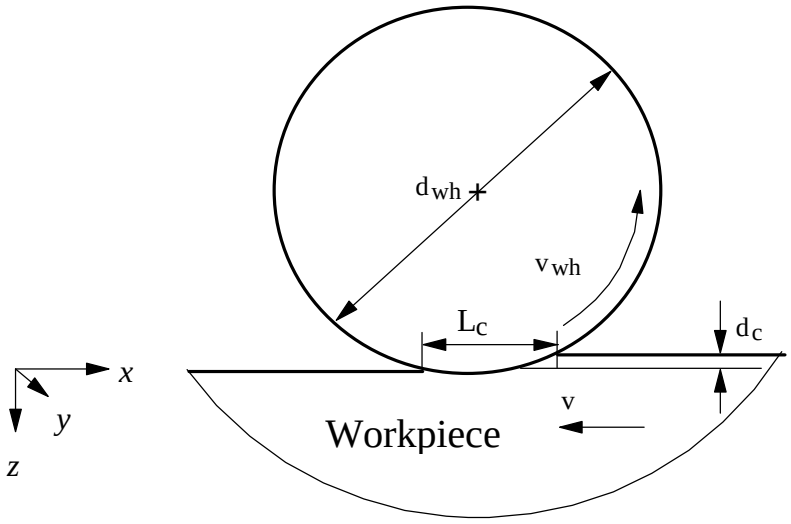

Figure 2.1 A grinding process geometry

In surface grinding, a wheel of diameter d_{wh} rotating with a peripheral velocity v_{wh} cuts a workpiece with nominal wheel depth of cut, d_c,. The workpiece moves with the grinding table speed, v that is much smaller than v_{wh}. As the grinding wheel cuts into the workpiece, it will be in

contact with the workpiece with an arc length of contact L_c. If the effect of deformation and motion of both the grinding wheel and the workpiece is neglected, L_c can be approximated as

$$L_c = (d_{wh}\ d_c)^{1/2} \quad 2.1$$

A grinding process can be classified as either an up- or down-grinding according to the moving direction of the grinding wheel relative to the workpiece. When the wheel velocity, v_{wh}, opposes the workpiece velocity, v, the process is said to be an 'up-grinding', otherwise it is called a 'down-grinding'.

As workmaterial is removed by wheel cutting, heat is generated thereby causing significant temperature rise in the wheel-workpiece contact zone, i.e., the grinding zone. The extent of the temperature rise relies on the workmaterial properties and the grinding conditions, such as material removal rate and coolant application.

2.2 Grinding Parameters

A grinding condition includes the setting in a grinding of the following parameters: type of grinding wheel, wheel speed, table speed, depth of cut, wheel dressing conditions and cooling conditions. For simplicity the above grinding conditions can be replaced equivalently with a different set of parameters suitable for modelling and computational purposes. In this context, according to Zhang et al. (1993), the profile of interaction stresses can be reasonably represented by a triangular profile. Accordingly, the heat generated by grinding is also approximated by a triangular heat source with peak q_a moving along the positive direction of x-axis on the workpiece surface (see Fig. 2.2b).

It should be noted that the peak of the mechanical traction force, p_a, coincides with that of the heat flux, i.e. q_a. The transient grinding temperature rise is calculated based on the heat flux intensity, q_a, the table speed reflected by the Peclet number, Pe, and the convection heat transfer coefficient, h. The moving traction force is replaced consistently by

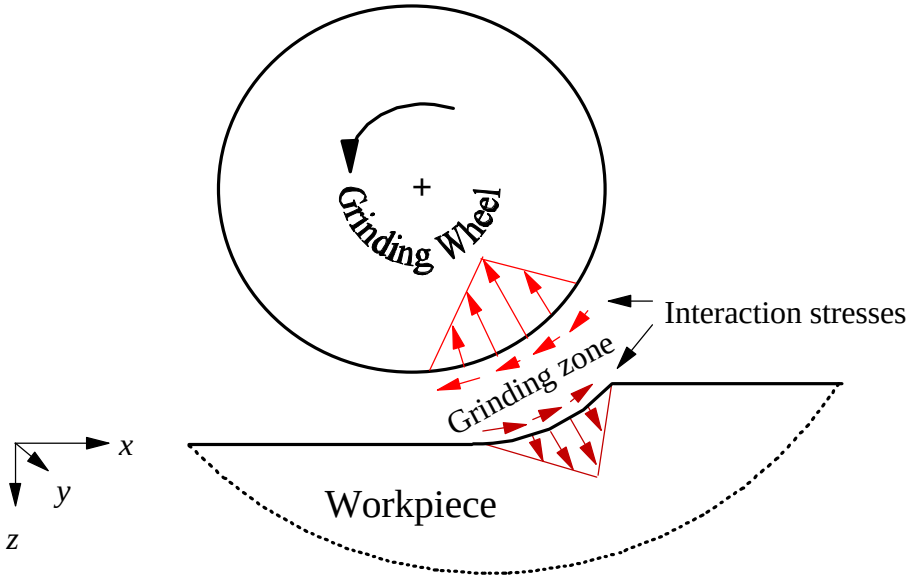

(a) the interaction stresses between a grinding wheel and a workpiece

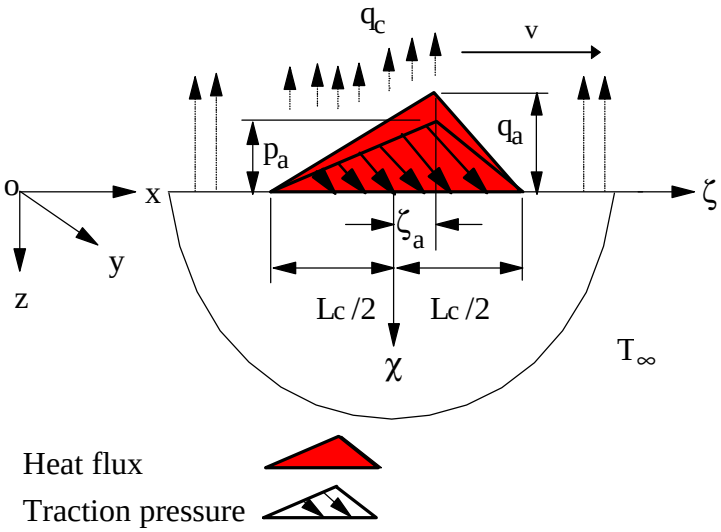

(b) the mechanics model of grinding

Figure 2.2 The modelling of grinding

normal and tangential forces with ratio μ

direction of the horizontal nodal force is governed by the type of grinding mechanism, which is

positive (in positive x-direction) for an up-grinding and negative (in negative x-direction) for a down-grinding. On the other hand, the locations of the traction peak, p_a, and the heat flux peak, q_a, must be different for the two types of grinding processes. According to Zhang et al. (1993) and Wager et al (1991), the relative peak location, as shown in Fig. 2.2b, is 0.25 for an up-grinding and 0.75 for down-grinding. To model the cooling effect of cooling fluid, a constant convection heat transfer coefficient is employed thus heat energy converted is linearly proportional to the relative grinding temperature, T.

The workmaterial considered in this study is EN23 steel with its chemical composition shown in Table 1 [British Iron and Steel Research Association, (1969)]. The dependence of workmaterial thermal properties on temperature is demonstrated in Fig. 2.3 and the thermo-mechanical properties are listed in Table 2. It is clear that thermal properties have a complex dependence on grinding temperature such that grinding temperature is in general a nonlinear function of the input heat flux intensity, q_a**.** Material properties can also vary with instant phase transformation. In the next section, we will discuss their modellings individually in more detail.

Table 1 The composition of EN23 steel

Composition (% weight)					
C	Si	Mn	Cr	Mo	Ni
0.32	0.25	0.55	0.71	0.06	3.41

Table 2 The thermo-mechanical properties of EN23 steel

Yield Stress (MPa)	Young's modulus (GPa)	Thermal coefficient of expansion (C^{-1})	Poisson's ratio υ
796	214	1.45×10^{-5}	0.27

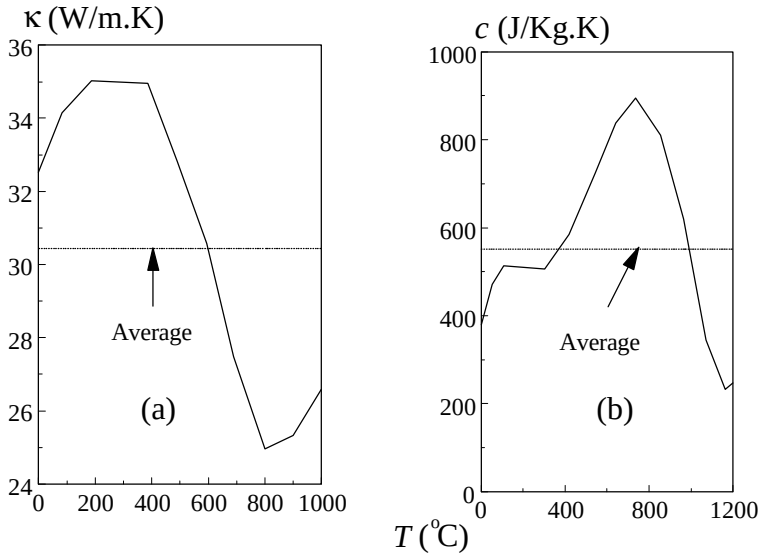

Figure 2.3 Temperature dependent thermal properties of EN23 steel
(a) thermal conductivity (b) thermal specific heat

2.3 Onset of Irreversible Deformation

The plastic yielding of a workpiece material subjected to grinding can be predicted by von Mises criterion:

$$(s_1-s_2)^2 + (s_1-s_3)^2 + (s_3-s_1)^2 = 2Y^2 \qquad 2.2$$

in which s_1, s_2 and s_3 are the principal stresses in the state of complex stress and Y denotes the yield stress of the material under a simple tensile test. Prior to yielding the stress tensor, $\boldsymbol{\sigma}$, is related to strain tensor, $\boldsymbol{\varepsilon}$, by elastic relationships characterized by an elastic constant stiffness (constant) matrix [Bathe (1982)], **D**, such that

$$\boldsymbol{\sigma} = \mathbf{D}\,(\boldsymbol{\varepsilon}-\boldsymbol{\varepsilon}_T) \qquad 2.3$$

where $\boldsymbol{\varepsilon}$ and $\boldsymbol{\varepsilon}_T$ are the iso-thermal strain and thermal strains tensors.

According to the von Mises yield criterion, the hydrostatic stress components have no influence on the effective stress defined by eq. (2.2). Thus a hydrostatic state of mechanical and/or thermal loading has no effect on the onset of yielding if its properties are independent of temperature variation or phase change.

2.4 Modelling of The Grinding Domain

A sufficiently large control volume must be used to simulate the semi-infinite domain in order to get reliable results by the finite element method. In this study, the boundary of the solution domain is not known in advance but has to be determined as a part of the solution and thus is said to be 'free' or 'open'. The term 'free-boundary problem' is commonly used when the boundary is stationary and when a steady state problem exists. Moving boundaries, on the other hand, are associated with time-dependent problems and the position of the boundary has to be determined as a function of time and space. In the cases of 'free' and 'open' boundaries two conditions are needed: (1) determination of the boundary itself and (2) completing the definition of the problem. For a grinding process, there are two sorts of boundary conditions, i.e. thermal and mechanical conditions. The open and free thermal boundary conditions are identified by a given ambient temperature (room temperature) ahead of the grinding zone and vanishing heat flux elsewhere. The open and free mechanical boundary conditions, on the other hand, are characterized either by vanishing displacement and stress conditions far from the grinding zone. To maintain a good approximation of the boundary conditions, appropriate control volumes need to be investigated in relation to grinding parameters and grinding zone length, L_c.

For a steady state process, open boundary conditions can be applied approximately by trying different control volume sizes and verifying the vanishing of the gradient of the boundary temperature, heat flux, stress and displacements prior to but close to the proposed geometric boundaries. To obtain a solution with thermal equilibrium, the grinding temperature ahead of the grinding zone should be equal to the ambient temperature and the displacements in the zone far away from the surface subjected to grinding must be zero. In a transient thermal approach,

however, the thermal equilibrium conditions should be maintained only at the furthest edge ahead of the grinding zone.

The geometry domain is discretized by isoparametric elements with more dense elements near the ground surface as shown in Fig. 2.4a. Equal elements are used in the first 1 mm depth as illustrated in Fig. 2.4b. This mesh style is used inclusively throughout this study. The details of each control volume size criterion are considered in the following relevant sections.

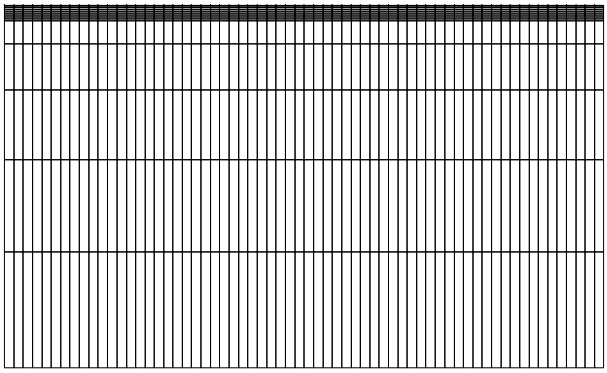

(a) whole model

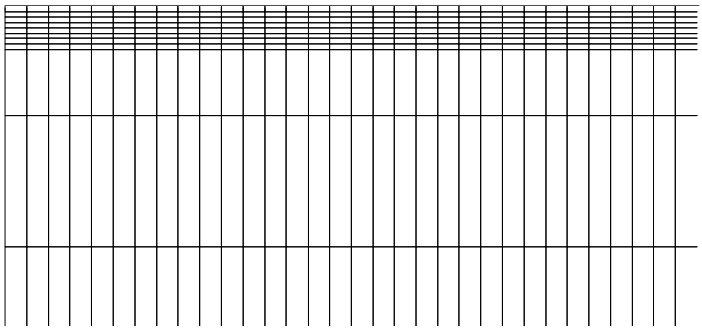

(b) surface elements

Figure 2.4 FEM mesh

The depth of elements is selected such that longer elements are generated near the depth of the control volume. The size of this particular control volume is $16L_c$ x $12L_c$. The element topography is built up by the help of the pre-processor of the ADINA system. Added to the 9 noded elements, 4 linear elements are used in some particular cases for simplicity and verification purposes.

2.4.1 Modelling of Thermal Boundary Conditions

As stated in Section 2.4, the grinding temperature rise and heat flux within the workpiece should vanish at the infinite boundaries. For steady state thermal grinding conditions, the boundary conditions ahead of the heat source require that both grinding temperature rise and heat flux be zero. With the aid of the analytical solution of moving band heat source [Jaeger (1942)], the steady state grinding temperature profiles are constructed in Fig. 2.5a. A wide range of the Peclet number from 0.125 to 8 is used. The selection of the constant band source for the boundary conditions associated with control volume size is essential for control volume accuracy as average conditions of load are assumed. It shows that as the dimension at the right hand side of the control volume increases a more accurate representation of right boundaries is achieved. To have a good grinding temperature solution in relation to the Peclet number a recommended right edge side is plotted in Fig. 2.5b.

It is clearly demonstrated that a larger right edge side needs to be considered if the Peclet number is smaller particularly when $Pe < 1$. In this study, the Peclet number range used is either equal or above 1 and the right side size is 4. The size of the left edge side, on the other hand, is decided by close examination of the temperature gradient back to the heat source location. Figure 2.5a shows that a good approximation of vanishing heat flux can be achieved if a right side size is more than $3L_c$. The validity of the control volume size is verified by investigating the analytical grinding temperature under different input heat flux profiles. Figure. 2.6a confirms that accurate control volume size is not much affected by the input heat flux as open boundaries are adequately modelled. For transient thermal grinding conditions, similar conditions apply only at the extreme left and right edges of the workpiece as stated earlier. The size of the control volume for a transient model should always be larger than that associated with the steady-state grinding process. To be more specific, the size of the transient control volume should be large enough to enclose the steady-state control volume thereby satisfying the free boundary conditions associated with the transient model as shown in Fig. 2.6b.

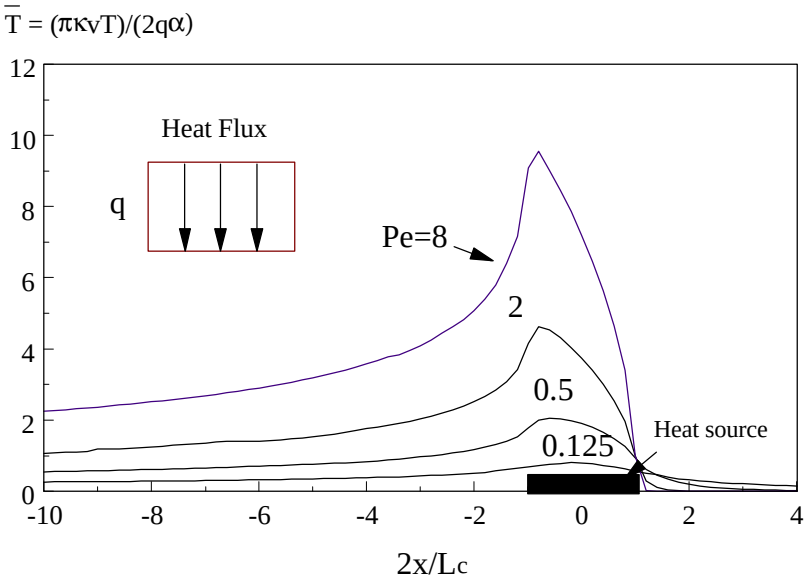

(a) dimensionless steady grinding

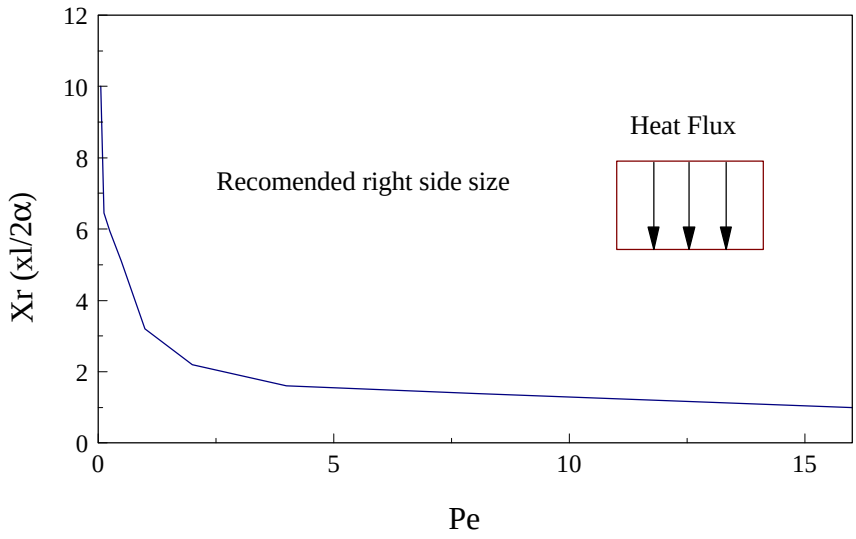

(b) minimum dimension at the right hand side of the control volume

Figure 2.5 Surface temperature of grinding

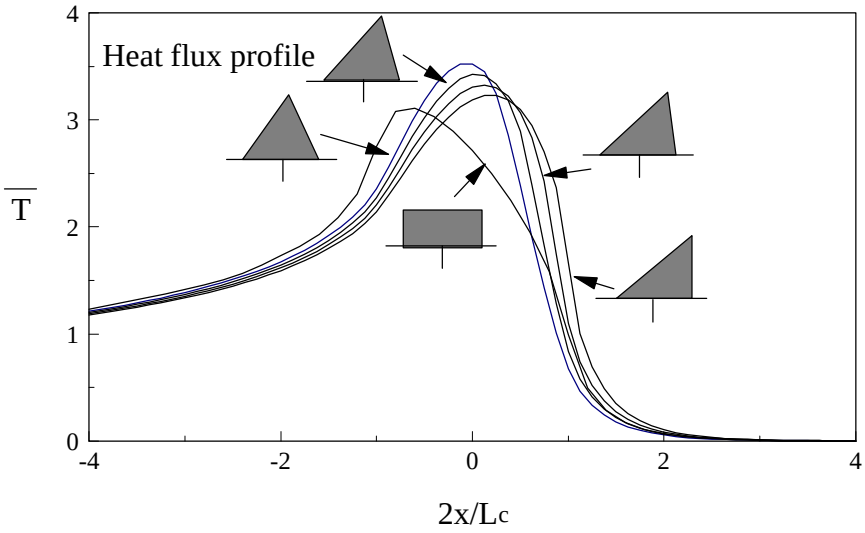

(a) the steady state temperature and heat flux

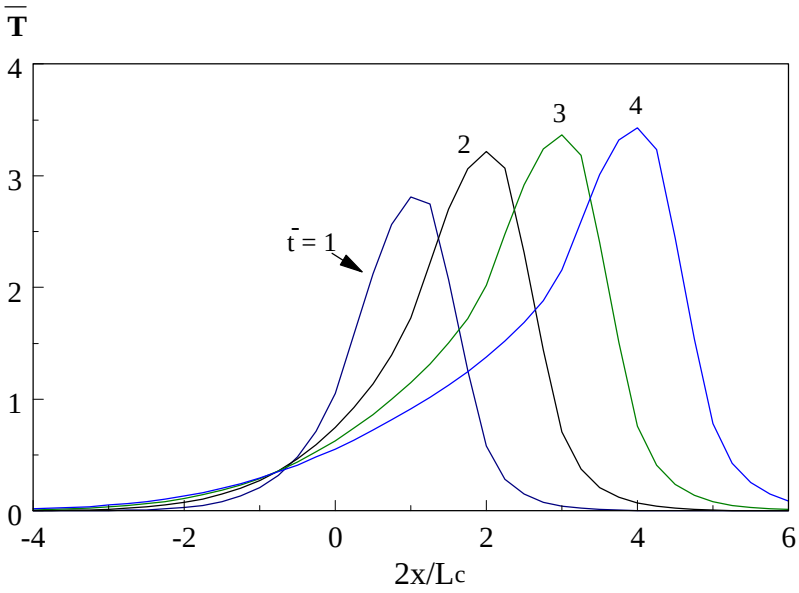

(b) the transient temperature

Figure 2.6 Dimensionless surface temperature (H=0, l_a=0.25, Pe=1)

Normally, a quasi-steady state grinding temperature in a workpiece can only be reached after the heat source has moved a large distance from the workpiece edge. Therefore the size of

the control volume of a transient FEM model must be sufficiently large. The accuracy of the steady-state grinding control volume is further examined by comparing the maximum numerical grinding temperature of different heat flux profiles with the relevant analytical solutions [Jaeger (1942)]. Figure 2.7 shows that a close agreement can be achieved when the Peclet number ranges from 0.5 to 8.

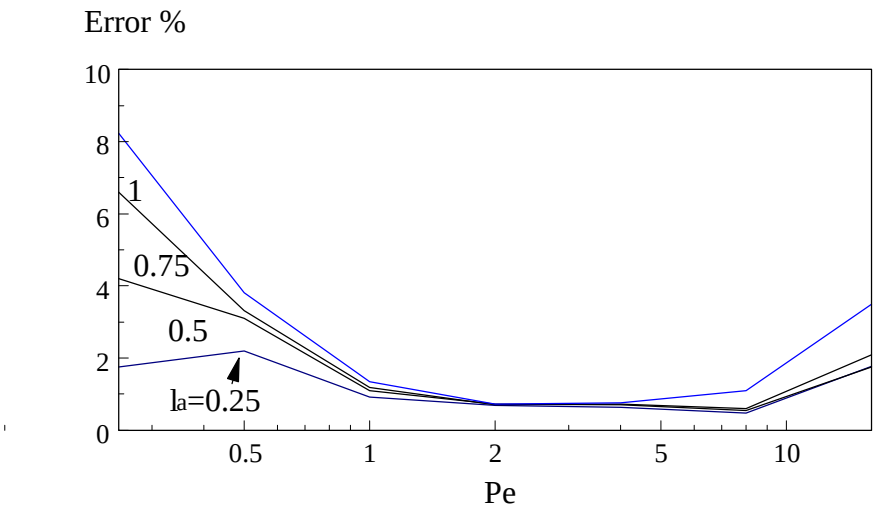

Figure 2.7 Error of maximum grinding temperature

Another measure of accuracy is considered by comparing the FEM solution of the transient grinding temperature with that of the analytical solution as demonstrated in Fig. 2.8. It is clear that the solutions agree in terms of both accuracy and stability. Moreover, the control volume size is adequate for free boundary modelling. The depth of the control volume is selected by inspection based on trial enlargement of the workpiece depth. For a given thermal analysis, a workpiece depth of 6 L_c (or more) is found to be accurate and reasonable for the given grinding conditions.

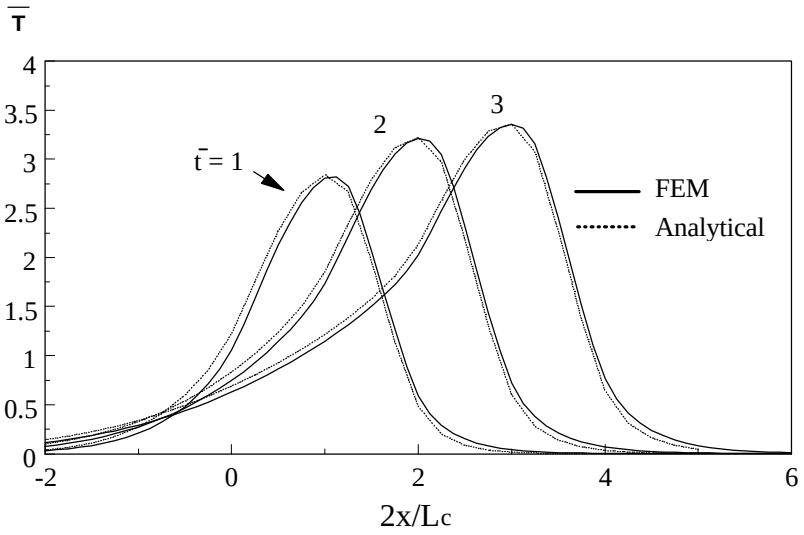

Figure 2.8 FEM transient grinding
vs analytical solution (Pe=1, l_a = 0.25,

2.4.2 Modelling of Mechanical Boundary Conditions

To reflect mechanical boundary conditions in grinding a careful consideration of the control volume size needs to be conducted. The grinding operation involves moving interaction forces and therefore is said to be a dynamic process. However, under a low table speed and with negligible vibrations of the grinding system, the process can be assumed as quasi-static. Added to the requirements of the thermal grinding process of the control volume size, the criterion of appropriate control size for an iso-thermal mechanical grinding operation needs to consider the free boundary conditions. In this context, free stress boundary conditions are used for the left and the right sides of the control volume. The total length of the workpiece is investigated by enlargement trials with vanishing displacements at the boundaries of the control volume. The depth of the control volume is investigated by considering different residual stress distributions such that stresses vanish at the bottom of the workpiece. In addition, the bottom of the workpiece is assumed rigid therefore no displacements are allowed.

2.5 Grinding Temperature

2.5.1 Governing Equations

For a large class of grinding operations, temperature distribution in the workmaterial may be calculated by solving the heat-conduction equation, subject to the geometrical and temperature boundary conditions. In general, the grinding temperature distribution, T, will depend on time, t. However, due to less significant inertia effects induced by a smooth change of grinding conditions, the problem may then be treated as a quasi-static one since the temperature distribution enters into the thermal-stress calculation as an integral load function [Boresi (1987)]. Accordingly, the temperature distribution may be expressed as follows:

$$T = T(x, y, z; t) \qquad 2.4$$

where (x,y,z) denote rectangular Cartesian coordinates and t denotes time. For a given time t, the above equation defines the grinding temperature distribution as a function of coordinates (x,y,z). For plane strain problems, the grinding temperature can be expressed as

$$T = T(x, z; t) \qquad 2.5$$

By the theory of heat conduction [Carslaw and Jaeger (1965)], the temperature, T, at a point in the workpiece is determined by the partial differential equation:

$$k \nabla^2 T + \frac{\partial k}{\partial T}\left(\left(\frac{\partial T}{\partial x}\right)^2 + \left(\frac{\partial T}{\partial z}\right)^2\right) = rc\frac{\partial T}{\partial t} \qquad 2.6$$

where ρ is the mass density; c is the specific heat energy and κ denotes the thermal conductivity. The room temperature properties of EN23 steel are shown in Table 3.

Table 3 The thermal properties of EN23 steel at room temperature

Thermal conductivity κ (W/m.C)	Specific heat capacity per unit volume, ρc (J/m$^{3)}$
32	2611985

2.5.1.1 Transient Problems

For workmaterial with temperature-dependent properties, a transient model needs to be utilized which in turn requires the simulation of heat source movement over a stationary workmaterial surface (z=0). Therefore the control volume needs to be attached to the fixed frame of reference (xoz) as shown in Fig. 2.2b. For a stationary frame of reference (xoz), the grinding zone boundary conditions are

$$\frac{\partial T}{\partial z} = \begin{cases} \frac{1}{k}\,(-q(x') + h\,T), & |\,x'\,| \le l,\ z = 0 \\ \frac{1}{k}\,(h\,T), & |\,x'\,| > l\ \ z = 0 \end{cases} \qquad 2.7a$$

with

$$T,\ \frac{\partial T}{\partial r} \to 0,\ when\ r \to \infty \qquad 2.7b$$

where $r=(x^2+y^2)^{1/2}$ and the input heat flux intensity is

$$q(x') = \begin{cases} \frac{q_p}{x_p + 1}\,(x'+1), & -1 \le x' \le x_p \\ \frac{q_p}{1 - x_p}\,(1 - x'), & x_p \le x' \le 1 \\ 0, & |x'| > 1 \end{cases} \qquad 2.7c$$

It is found that transient approaches do need a large number of time steps to reach the steady state conditions required. Thus much more computational time is needed. However, if the workmaterial properties are temperature-independent the steady state approach may be employed efficiently as will be discussed in the following section.

2.5.1.2 Steady State Problems

If the workmaterial properties are constant, eq. (2.6) can be simplified to

$$k \nabla^2 T = rc \frac{\partial T}{\partial t} \qquad 2.8$$

If the reference frame is moving with a constant table speed, v, eq. (2.8) can be simplified to a two-dimensional steady state grinding process such that

$$\frac{\partial^2 T}{\partial x'^2} + \frac{\partial^2 T}{\partial z'^2} + \frac{v}{a} \frac{\partial T}{\partial x'} = 0 \qquad 2.9$$

However the available equations that can be solved by ADINA are of the form

$$\frac{\partial}{\partial x'} \mathrm{K}(x') + \mathrm{K}(x') \frac{\partial^2 T}{\partial x'^2} + \mathrm{K}(x') \frac{\partial^2 T}{\partial z'^2} = 0 \qquad 2.10$$

with the boundary conditions

$$\frac{\partial T}{\partial z} = \frac{1}{\mathrm{K}} (-Q(x')) \ , \ z = 0 \qquad 2.11$$

where x'=x-v×t, z'=z, K(x') is the thermal conductivity and Q(x') is the input heat flux at x'. When compared with eq. (2.9), eq. (2.10) may yield the same temperature solution if

$$\frac{1}{c v} \left(\frac{d \mathrm{K}}{d x'} \right) = \frac{\mathrm{K}}{k} \qquad 2.12$$

The integration of eq. (2.11) yields

$$K = k_o \exp\left(\frac{v\,x'}{a}\right) \qquad 2.13$$

where k_o is a non-zero integration constant. Substituting of eq. (2.13) into eq. (2.10) yields

$$k_o \exp\left(\frac{v\,x'}{a}\right)\left(\frac{\partial^2 T}{\partial x'^2} + \frac{\partial^2 T}{\partial z'^2} + \frac{v}{a}\frac{\partial T}{\partial x'}\right) = 0 \qquad 2.14$$

Since the first term of eq. (2.14) is non-vanishing, the second term should be zero which precisely yields the same equation as (2.9). To obtain the same temperature gradients as eq. (2.9), Q(x') should be

$$Q(x') = \begin{cases} \frac{K}{k}\left(-q(x') + h\,T\right), \; |x'| \le l, \; z = 0 \\ \frac{K}{k}\left(h\,T\right). \; |x'| > l \;\; z = 0 \end{cases} \qquad 2.15$$

therefore surface temperature gradient yields

$$\begin{cases} \frac{\partial T}{\partial z} = \begin{cases} \frac{k_o}{k}\left(-q(x') + h\,T\right)\exp\left(\frac{v\,x'}{a}\right), \; |x'| \le l, \; z = 0 \\ \frac{k_o}{k}\left(h\,T\right)\exp\left(\frac{v\,x'}{a}\right), \; |x'| > l \;\; z = 0 \end{cases} \\ T, \; \frac{\partial T}{\partial r} \to 0, \; when \; r \to \infty \end{cases} \qquad 2.16$$

Correspondingly, the relevant boundary conditions (2.16) should be used to replace (2.7) when ADINA is used for the grinding problem with a moving heat source.

2.6 Phase Transformation

The rapid heating and cooling in a grinding process may cause phase transformation and thermal plastic deformation simultaneously in a workpiece and in turn introduce substantial residual stresses. When phase transformation occurs, the properties of the workpiece material will change. The extent of such change depends on the temperature history experienced and the instantaneous thermal stresses developed. To carry out a reliable residual stress analysis, therefore, a comprehensive modelling technique and a sophisticated computational procedure that can accommodate the property change of material need to be developed.

2.6.1 Critical Grinding Temperature History

The following relationships associated with critical conditions of phase transformations are all based on the chemical composition of the workmaterial in percentage [Atkin and Met (1977)]. To initiate the phase change in the austenised ground components, a critical cooling rate between Ac1 (C) and 500 C should be equalled or exceeded

$$Ac1\ (C) = 723 - 20.7\ Mn - 16.9\ Ni + 29.1\ Si + 16.9\ Cr \qquad 2.17$$

where Mn, Ni, Si and Cr are the percentage of these elements.

The critical cooling velocity to be equalled or exceeded in order to obtain a martensitic transformation relies on the chemical composition. Alternatively, the maximum critical cooling time, denoted as t_c, that should not be exceeded to have martensite is expressed as:

$$\log_{10}(t_c) = 3.27\ C + 0.05\ Si + 0.63\ Mn + 0.71\ Cr + 0.52\ Mo + 0.03\ Ni - 1.818 \qquad 2.18$$

According to the chemical composition and eqs. 2.17-18, the critical conditions for martensite transformation to take place are summarized in Table 4. Typical critical grinding temperature histories are shown in Fig. 2.9.

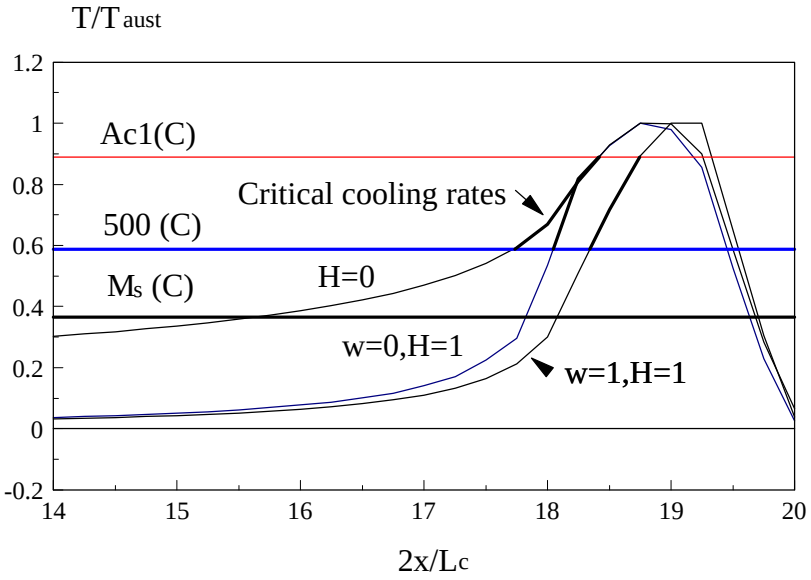

Figure 2.9 A typical example of critical grinding temperature history, showing the combined effects of cooling factor, w, convection heat transfer coefficent, H, (Pe=1, l_a =0.25)

It is found that the maximum surface temperature in grinding is initially elevated to an austenising temperature. During the cooling process different cooling times were observed between Ac1 and 500 ^{o} C depending on grinding conditions. The surface cooling mechanism with convection heat transfer has a faster cooling time than that of dry grinding (H=0). The cooling factor, w, has a minor influence on the critical cooling time.

Table 4 The phase change properties of EN23 steel

Critical Cooling time between 1029 K and 773 K	Austenizing temperature (K)
< 1.6 sec	1123

2.6.2 The Constitutive Relations of Phase Transformation

We propose the following constitutive model which describes the transformation plasticity accompanying strain-induced martensitic transformation in steel alloys. Here, phase transformation is assumed to be temperature-history-dependent only, therefore the steel composition is used to determine the variation of workmaterial hardness Hv of the finally formed martensite [Atkin and Met (1977)]:

$$HV = 463.2376 + 21 * \log(Cr_{700}) \qquad 2.19$$

where Hv is the Vickers hardness defined as the load divided by the surface area of a square diamond pyramid indentation with top angle of 136 degrees with the indentor being regarded as a rigid body. Cr_{700} in the equation is the cooling rate in degrees per hour at 700 ^{o}C. The yield stress of martensite, M_Y, can be calculated as

$$M_Y = 80. + 2.7544 * HV \qquad 2.20$$

The progress of the martensite transformation is found to be dependent on the starting temperature of martensite formation, M_s, and the final temperature, M_f, as shown in Fig. 2.10. According to the composition of EN23, M_f is 300 ^{o}C while M_s is 850 ^{o}C.

The yield stress of workmaterial undergoing phase transformation is assumed as a weighted averaged quantity based on the percent of martensite formed, M%, that is

$$s_Y = M\% * M_Y + (1 - M\%) * Y \qquad 2.21$$

where s_Y is the instantaneous yield stress of the ground components undergoing phase change during grinding and M% is the percentage of martensite formed. The other properties are considered the same as that of the original workmaterial.

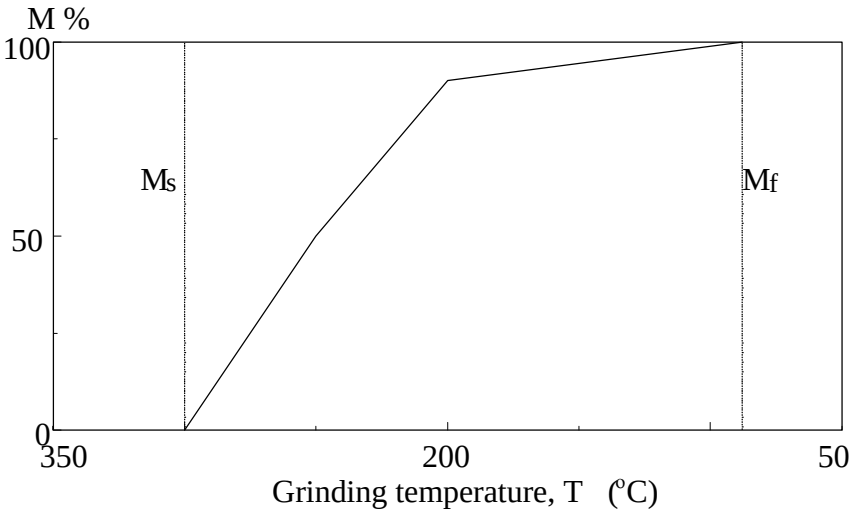

Figure 2.10 Quantitive phase change and cooling grinding temperature

As martensite forms a maximum volume increase of 4.3% is anticipated to develop [Reed-Hill (1964)]. The progress of volume change is directly related to the martensite percentage, *M*%, thus the maximum volume growth is anticipated for 100 % phase change.

Practically, the volume growth in a component during grinding is resisted by the compressive stress developed by the parts of workpiece material that are without phase change. Consequently, martensite volume growth is a key factor in grinding stress history and in residual stress distributions. In the given analysis, the volume growth is imposed by employing a negative thermal coefficient of expansion, α, during critical cooling such that plane-strain conditions are maintained. Numerically, this is modelled by dividing the total volume growth into one component in x-direction and the other one in z-direction. Since the volume strain is associated with grinding temperature change, the temperature drop is calculated first. Secondly, the negative component of the thermal coefficient is calculated to keep the desired volume strain. The thermal coefficient of expansion is evaluated independently for each integration point of the finite elements undergoing phase and volume change.

2.7 Implementation of ADINA Code

2.7.1 Development of User-Subroutines

According to the ADINA system and for the convenience of the code user, there exist a variety of options that enable special codes for workmaterial and boundary conditions to be built up. In this study, the grinding heat generated in the grinding zone together with the moving interaction forces, the workmaterial properties, the cooling power of cooling fluid, are simulated to model the grinding temperature, the interaction pressure between the grinding wheel and the workpiece and the resulting residual stresses. Accordingly, three major codes are developed in FORTRAN language.

2.7.1.1 Grinding Zone Heat Source and Convection Mechanism

The main advantage of the material model developed below is its applicability in terms of solution stability and computational cost. The model can be used for general moving boundary conditions associated with moving heat sources. As stated in Section 2.1, the material model is defined by a user-supplied code written in FORTRAN and inserted into CUSER2 and CUSERH subroutines. It is then compiled and linked to other object files for program execution. This model expresses grinding conditions and thermal properties in terms of materials parameters of both temperature-independent and temperature-dependent properties.

2.7.1.2 Consistent Nodal Force in Grinding Zone

Referring to Section 2.1, the function of the grinding wheel could be macroscopically replaced by a set of equivalent moving stresses. Here, we use the triangular model for the interface stresses proposed by Zhang et al. (1993). Since the size of the grinding zone is much smaller compared with the dimensions of the workpiece itself, the workpiece could be approximated as a semi-infinite domain. Nevertheless, the moving surface stresses should make up the same

resultant grinding force. When using the finite element method [Bathe(1982)] therefore, the following relation must hold in the direction normal to the workpiece surface:

$$F_i = \sum_{n=1}^{e} \int_{-1}^{+1} N_i^n \, P(h) dh \, , \qquad 2.22$$

where F_i is the ith normal nodal force applied on the ith node, N_i^n is the ith interpolation function associated with the nth element, e is the total number of surface elements, $\eta=2(x-vt)/L_c$ is a parameter indicating the instant position of the moving stresses, x is a coordinate variable shown in Fig. 2.1, v is the table speed, t is time and P is the distribution function of the normal stress defined by

$$P = \begin{cases} \dfrac{(h+1)}{(l_a+1)} P_a \, , & -1 \le h \le l_a \\ \dfrac{(h-1)}{(l_a-1)} P_a \, , & l_a \le h \le 1 \\ 0. & |h| > 1 \end{cases} \qquad 2.23$$

In eq. (2.23), P_a is the peak value of the normal stress profile and $l_a = 2x_a/L_c$ indicates the relative apex position in the grinding zone. It is assumed that the horizontal shearing stress is proportional to the normal one by a constant factor μ. Therefore on the ith node the nodal shearing force is

$$T_i = m F_i \, , \qquad 2.24$$

where μ is a constant ratio whose sign denotes the type of grinding mechanism (i.e. negative for down-grinding and positive for up-grinding). The simulation of the movement of surface stresses and workmaterial properties is implemented by employing the user-defined input loading options (USERL) of ADINA system as coded in Appendix B. Typical consistent force profiles are shown in Fig. 2.11. For a larger number of elements, more nodal forces are required but with lower intensity. The increase of surface elements may improve the solution accuracy as smoother stress distribution may be achieved but at the cost of computational time. In this study, four

quadratic elements (see Fig. 2.11b) are used inclusively. In some cases the number of surface elements is doubled to check the solution accuracy in terms of residual stresses.

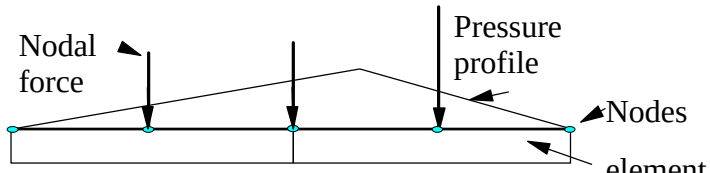

(a) 2 quadratic elements in the grinding

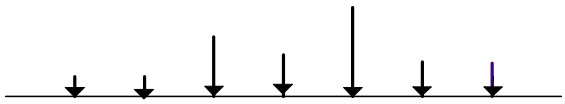

(b) 4 quadratic elements in the grinding

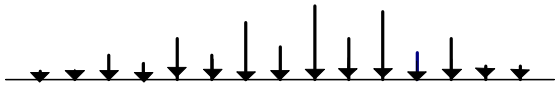

(c) 8 quadratic elements in the grinding

Figure 2.11 Consistent nodal forces and FEM boundary mesh size

2.7.1.3 Constitutive Matrix of Elastic-Perfectly-Plastic Material

According to Prandtl-Reuss elastic equations of plastic flow, the stress and strain increments are related by a proportional factor reflected by the stiffness matrix. The constitutive matrix, **D**, of an elastic-perfectly plastic workmaterial can be divided into two parts, namely elastic and elastic-plastic , i.e.

$$\mathbf{D} = \mathbf{D}^e - \mathbf{D}^p \qquad 2.25$$

The elastic matrix, $\mathbf{D}^e$, is

$$\mathbf{D}^e = 2G\begin{Bmatrix} \frac{1-n}{1-2n} & \frac{n}{1-2n} & \frac{n}{1-2n} & 0 \\ \frac{n}{1-2n} & \frac{1-n}{1-2n} & \frac{n}{1-2n} & 0 \\ \frac{n}{1-2n} & \frac{n}{1-2n} & \frac{1-n}{1-2n} & 0 \\ 0 & 0 & 0 & \frac{1}{2} \end{Bmatrix} \qquad 2.26$$

and the elastic-perfectly plastic matrix is

$$\mathbf{D}^p = \frac{3G}{Y^2}\begin{Bmatrix} s_{xx}^d s_{xx}^d & s_{xx}^d s_{yy}^d & s_{xx}^d s_{zz}^d & s_{xx}^d s_{xy} \\ s_{yy}^d s_{xx}^d & s_{yy}^d s_{yy}^d & s_{yy}^d s_{zz}^d & s_{yy}^d s_{xy} \\ s_{zz}^d s_{xx}^d & s_{zz}^d s_{yy}^d & s_{zz}^d s_{zz}^d & s_{zz}^d s_{xy} \\ s_{xx}^d s_{xy} & s_{yy}^d s_{xy} & s_{zz}^d s_{xy} & s_{xy} s_{xy} \end{Bmatrix} \qquad 2.27$$

where ν is the Poisson ratio, G is the shear modulus, Y is the yield stress and σ^d is the deviatoric component of a stress defined as:

$$s_{bb}^d = s_{bb} - (s_1 + s_2 + s_3)/3 \qquad 2.28$$

2.7.2 Generation of Input Data

To provide a step-by-step procedure for the preparation and checking of the input data for ADINA using ADINA-IN, a number of guidelines are presented primarily in Appendix C to help the reader to become familiar with basic commands necessary for creating a complete model. For further information on the theoretical basis of ADINA, 'Theory and Modeling Guide' [ADINA R&D (1992)] needs to be considered.

2.8 FEM Accuracy and Error analysis

In the next section, the solution accuracy and stability of some typical grinding temperature and residual stress problems are investigated by different approaches depending on the grinding conditions

2.8.1 Grinding Temperature

Here more attention is paid to the accuracy of the grinding temperature calculation of a workpiece with temperature-dependent properties. A workpiece with a linear dependence of thermal properties on grinding temperature is selected as the workmaterial [Isenber and Malkin,(1975)]. For simplicity the results from the transient thermal analysis are compared with those of the steady state approach on the basis of the large movement of a banded heat source over the ground surface. Typical results are shown in Figs. 2.12 and 13. In Fig. 2.12 the specific heat capacity is taken as constant while in Fig. 2.13 both thermal conductivity and specific heat capacity are linear functions of grinding temperature. The comparison shows remarkable agreements particularly under a high Peclet number, e.g., Pe=5.

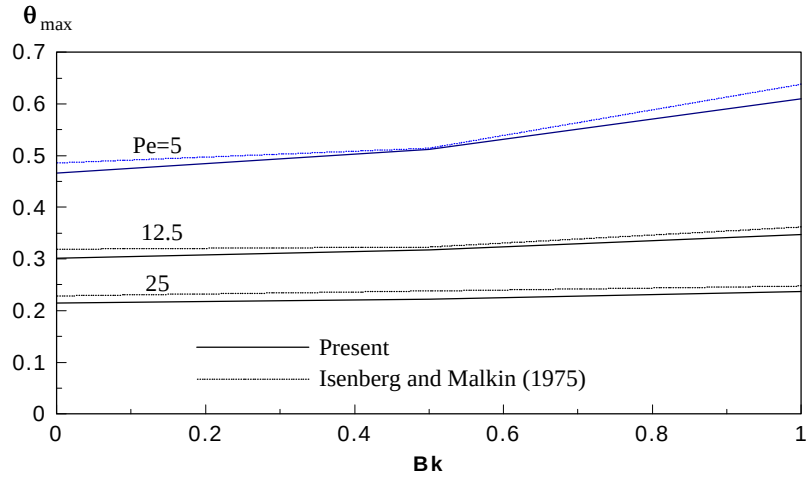

(a) Bc=0

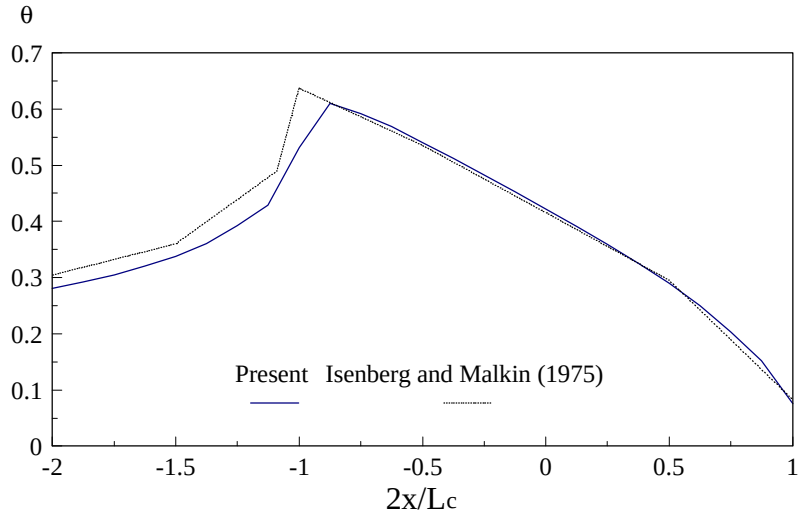

(b) Bc=0, Bk=1, Pe=5

Figure 2.12 Grinding surface temperature with temperature dependent material properties

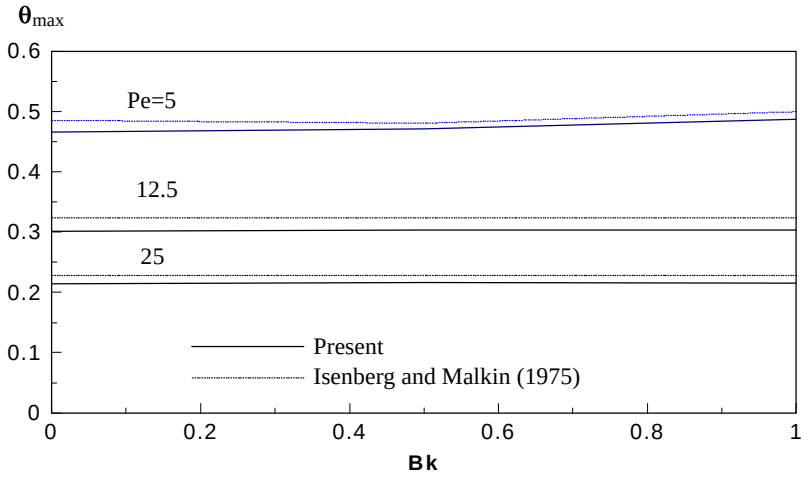

(a) Bc/Bk=2.3

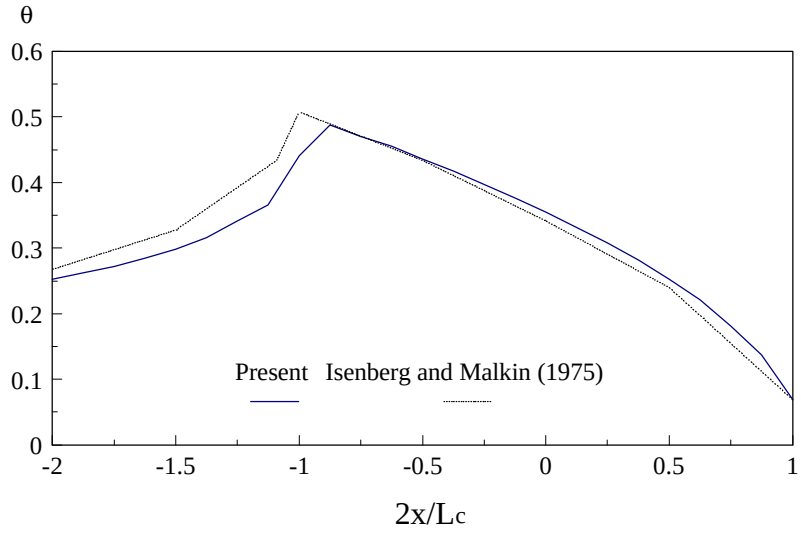

(b) Bc=2.3, Bk=1, Pe=5

Figure 2.13 Grinding surface temperature with temperature dependent material properties

2.8.2 Grinding Stresses

For the sake of reliability, the numerical solutions obtained by the finite element method need to be tested and verified. Prior to plastic deformation, numerical solution accuracy is verified by comparing the maximum von Mises stress (effective stress σ_e) with the analytical solution [Johnson (1985)] of an elastic semi-infinite plane subjected to a normal and a shearing stress on its surface over the interval $-L_c/2 \le x \le L_c/2$. The finite element mesh used is that of Fig. 2.4. Figure 2.14 shows that the finite element method gives very good predictions. Therefore the mesh discretization of Fig. 2.4 is acceptable for thermal analysis.

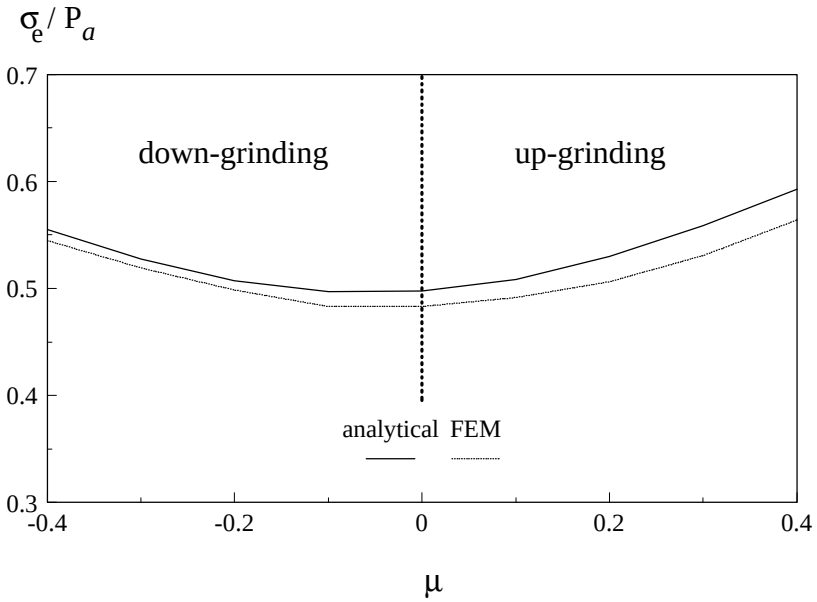

Figure 2.14 Analytical *vs* FEM elastic solution
(l_a =0.25, $2z/L_c$ =0.375)

Beyond elastic deformation the analytical solutions of stresses are no longer of beneficial use. Therefore a different technique is used for the examination of solution accuracy. One major source of solution errors is the approximation imposed by the finite element discretization which can be investigated by analyzing different mesh sizes and topography. Here, the variation of the residual stress solution with the change of surface element numbers is examined in Fig. 2.15. It is clear that a further finer mesh beyond 64 surface elements (i.e. 128 surface elements) brings

about very little variation of solution and therefore is not recommended in terms of computational efficiency.

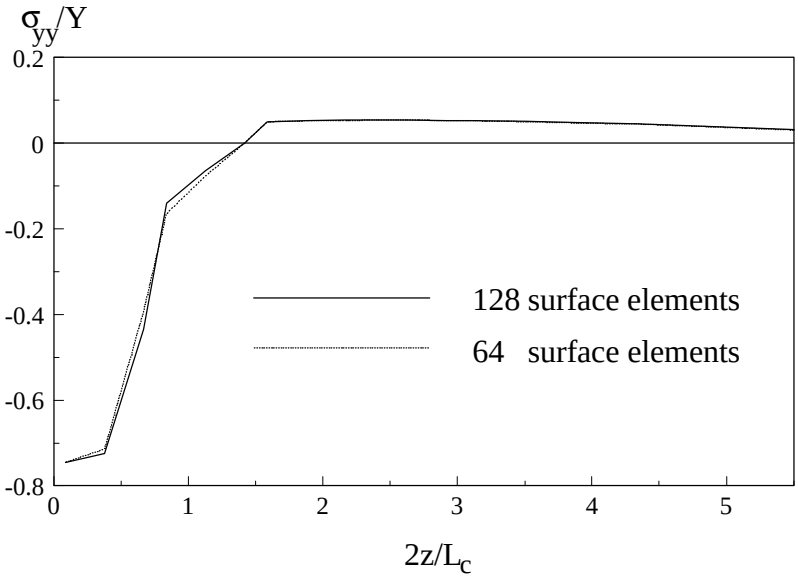

(a) plane stress

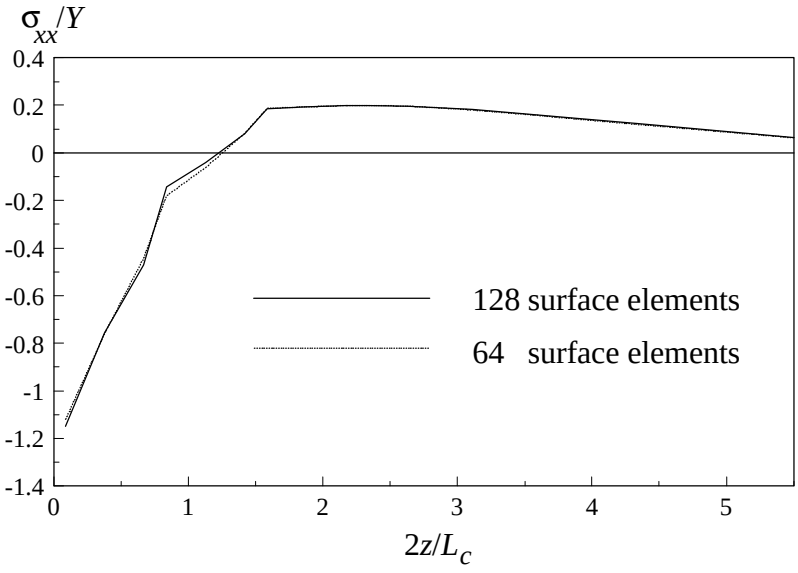

(b) longitudinal stress

Figure 2.15 Effect of mesh refinement on residual stresses (p_a =2.5 Y, μ=-0.4, l_a =0.25)

For thermal stress solutions of a workmaterial with constant properties, similar approaches of mesh refinement in z-direction are employed. Figure 2.16 compares the effect of element number doubling across the workpiece depth in the first mm layer.

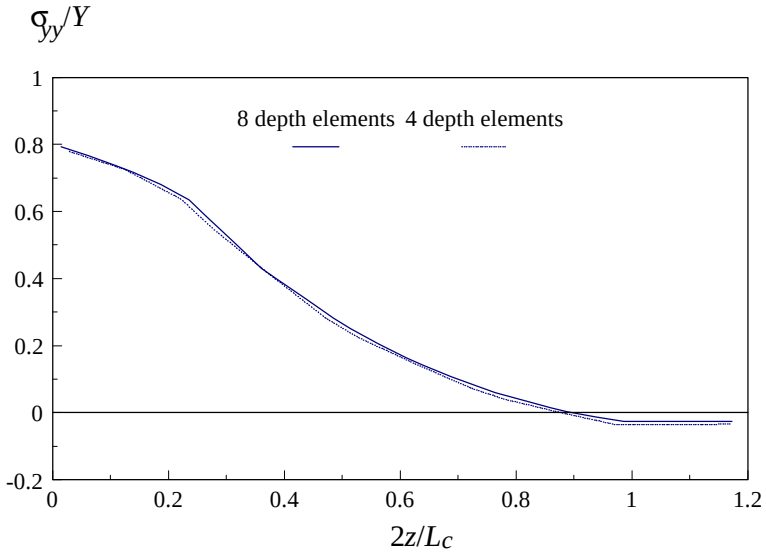

(a) plane stress

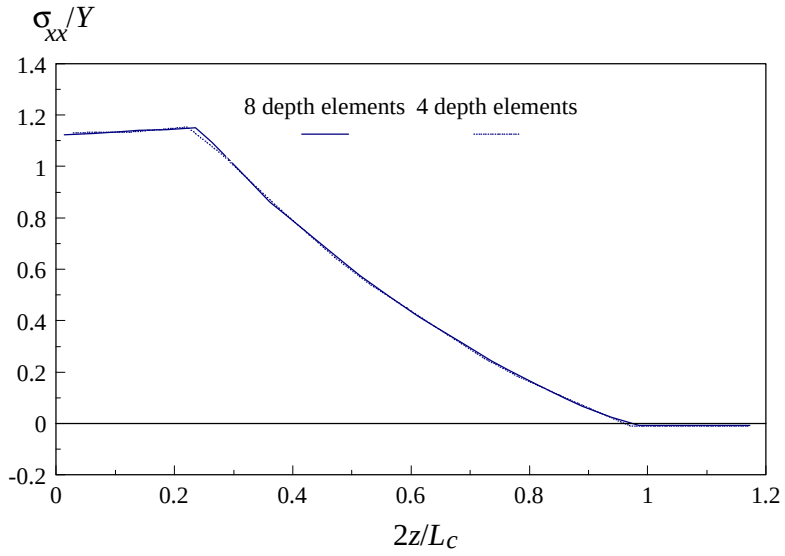

(b) longitudinal stress

Figure 2.16 Error analysis of thermal residual stress (q_a=40 MW/m^2, Pe=1, H=0, l_a=0.25)

The results show that there is only a slight influence of mesh refinement on thermal residual stress distribution. Therefore a surface layer of 1 mm with 4 divisions is economical.

With critical grinding temperature history, phase change in a workpiece material may take place. This is usually accompanied by a change of workmaterial properties in a very thin surface layer. Therefore, a finer FEM mesh may be needed for a smooth modelling of phase change and resultant residual stresses. Figure 2.17 shows the effect of surface layer depth divisions on the solution accuracy and indicates that surface divisions above 8 linear elements do not change the residual stress distribution critically. However, more element division along the depth can slightly improve the phase transformation prediction and the change of workmaterial properties but at the cost of much longer computational time. Thus surface linear elements with 8 depth divisions can reasonably model the phase change at a lower computational cost.

To verify the accuracy of the user-defined subroutine required for phase transformation and general change of workmaterial properties, a comparison is performed against the relevant numerical solution of the standard elastic-plastic code of the ADINA system as shown in Figs 2.18 and 2.19. Although the user-defined code uses an explicit stress integration scheme, both longitudinal and plane stresses are in close agreement with those of standard ADINA under thermo-mechanical grinding conditions. The effect of stress increment subdivisions on the solution stability of the user-defined code is further investigated as shown in Fig. 2.19. It shows that the solution accuracy of the explicit code increases as more increment subdivisions are employed. For numerical efficiency, a maximum of twenty subdivisions of stress increments are used throughout the relevant calculations of grinding simulation. Furthermore, the subdivisions of stress increments are performed only for those parts where plastic deformation occurs to save the CPU computational time.

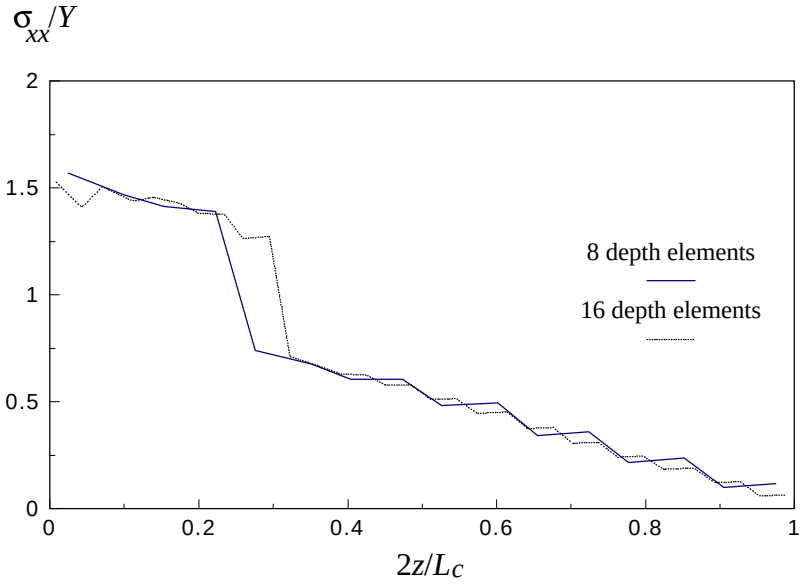

(a) longitudinal stress

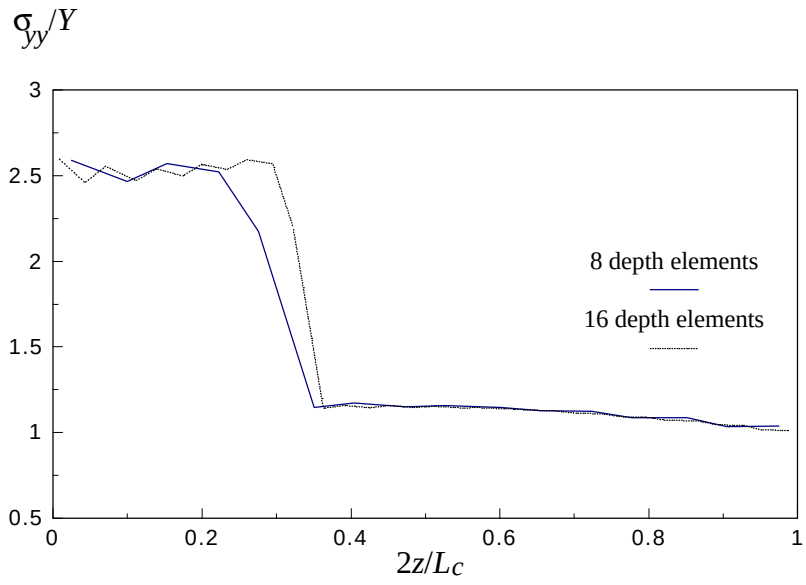

(b) plane stress

Figure 2.17 Error analysis of phase change induced residual stresses (q_a=80 MW/m2, Pe=1, H=0, l_a=0.25)

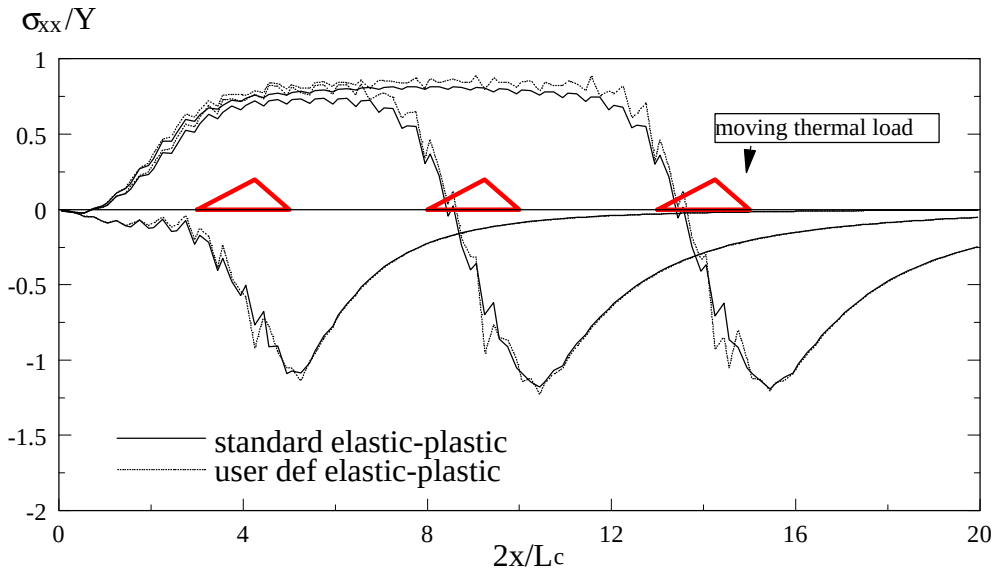

(a) longitudinal thermal stress (q_a =80MW/m^2 , Pe=1, H=0, l_a=0.25)

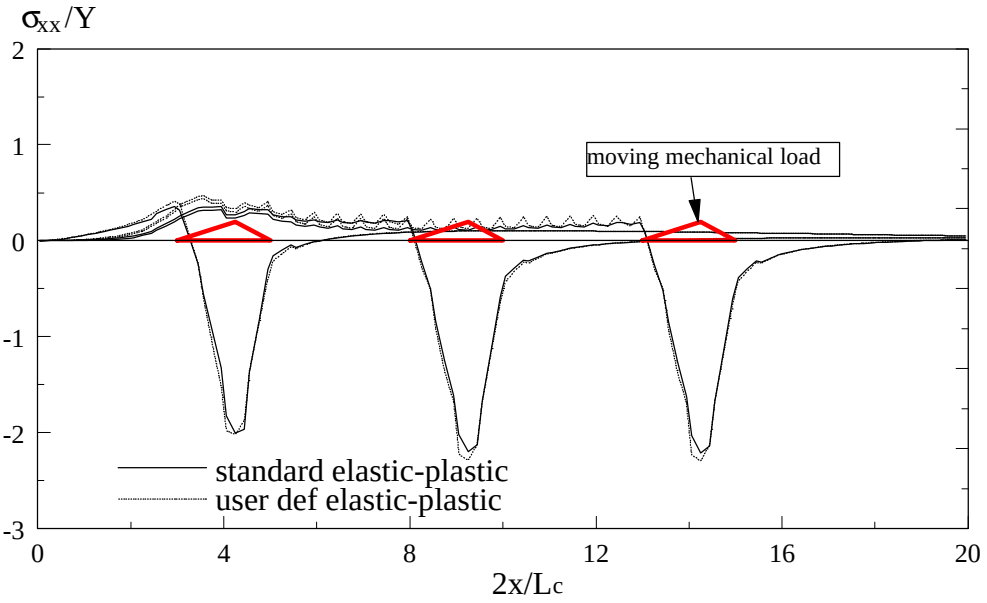

(b) longitudinal mechanically induced stress (p_a=2Y, μ=0.1, l_a=0.25)

Figure 2.18 User supplied code and standard ADINA code of elastic-perfectly plastic material (no stress increment divisions)

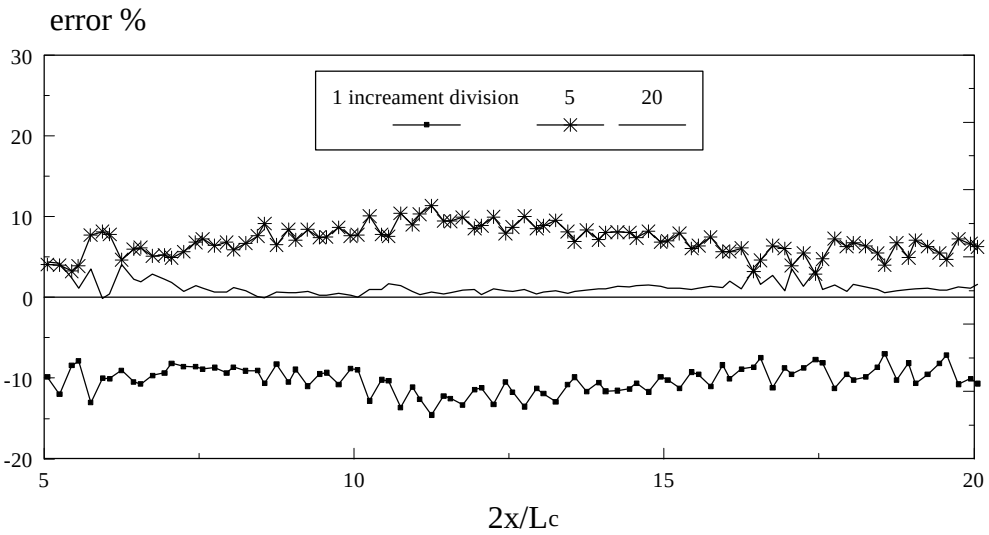

Figure 2.19 A typical stability analysis of surface σ_{xx} using the user-supplied code (elastic-perfectly-plastic material)
(p_a =2Y, μ=0.1, l_a=0.25, H=0, Pe=1, q_a= 80MW/m²)

2.9 Summary

A comprehensive methodology for modelling grinding conditions and associated boundary conditions was presented. The individual modelling techniques to explore each of the residual stresses mechanisms were discussed. Grinding conditions were identified by a set of grinding parameters. Key problems associated with boundary condition descriptions were addressed in relation to the grinding conditions. The grinding temperature and its modelling aspects were discussed in detail. The phase change and the relevant constitutive relations associated with the critical grinding temperature history were considered. For a proper simulation of the grinding conditions the implementation of the ADINA code was demonstrated. Finally, an error analysis was conducted to test the accuracy and the stability of the developed model. The modelling techniques developed in this chapter lay the foundation for further analysis in this thesis.